

We are IntechOpen, the world's leading publisher of Open Access books Built by scientists, for scientists

6,900

Open access books available

186,000

International authors and editors

200M

Downloads

Our authors are among the

154

Countries delivered to

TOP 1%

most cited scientists

12.2%

Contributors from top 500 universities



WEB OF SCIENCE™

Selection of our books indexed in the Book Citation Index
in Web of Science™ Core Collection (BKCI)

Interested in publishing with us?
Contact book.department@intechopen.com

Numbers displayed above are based on latest data collected.
For more information visit www.intechopen.com



Colloidal Photonic Crystals Containing Copper-Oxide and Silver Nanoparticles with Tunable Structural Colors

Chun-Feng Lai

Additional information is available at the end of the chapter

<http://dx.doi.org/10.5772/65007>

Abstract

In this chapter, we investigated polystyrene (PS) colloidal photonic crystal (CPhC) color films containing copper-oxide (CuO) nanoparticles (NPs) and silver (Ag) NPs and exhibiting tunable structural colors. PS CPhC color films containing CuO-NPs and Ag-NPs were prepared through thermal-assisted self-assembly by using a gravitational sedimentation method. Doped CuO-NPs and Ag-NPs deposited on the bottom of the substrate and acted as black materials that absorb background and scattering light. Experimental results showed that brilliant structural colors were enhanced because of the absorption of incoherently scattered light, and color saturation was increased by the distribution of metal NPs on PS CPhC surfaces. The brilliant structural colors of CuO-NPs/PS and Ag-NPs/PS hybrid CPhC color films were based on the scattering absorption and Bragg diffraction theory. The reflection peaks of metal-NPs/PS hybrid CPhCs and pure PS CPhCs were measured by UV-Visible reflection spectrometry and theoretically calculated based on the Bragg diffraction law. Additionally, the structural colors of metal-NPs/PS hybrid CPhC color films were assessed through color measurements based on the Commission International d'Eclairage 1931 standard colorimetric system. Finally, this chapter exhibits a simple method to generate tunable structural color of functional materials for numerous applications, such as in textile fabrics, bionic colors, catalysis, and paint.

Keywords: colloidal photonic crystals, copper-oxide, silver, nanoparticles, structural colors

1. Introduction

Structural colors generated by nanostructures are generally classified as iridescent [1–3] and non-iridescent colors [4–7]. The brilliant iridescent character of nanostructures has attracted

considerable attention for a variety of applications [8–10]. Iridescent colors produced by interference, diffraction, or light scattering are generated by periodic lattice crystals. Colloidal photonic crystals (CPhCs) of periodic crystals, which can reflect light at a specific photonic band gap (PBG) caused by periodic variation of refractive index in crystal structures [11, 12], are artificially fabricated. Polystyrene (PS), SiO_2 , or polymethyl methacrylate (PMMA) nanospheres of 3D CPhCs were generally fabricated by a self-assembly method [13–15]. 3D CPhCs still have several problems which limit the applications, containing low color visibility (opalescent appearance) and poor crystal quality.

The structural color of CPhCs is extremely dull because of the interferences of scattering and background light (**Figure 1(a)**). An effective method to address low color visibility is to mix highly absorbent black materials in the visible light region into colloidal systems to enhance color saturation, because black materials can reduce incoherent scattering to enhance color [16–19] (**Figure 1(b)**). Carbon black (CB) [20–23], carbon [24, 25], carbon-modified colloidal nanospheres [26, 27], and metal nanoparticles (NPs) [28–32] of black materials as additives have been recently used to fabricate CPhCs that exhibit enhanced structural colors.

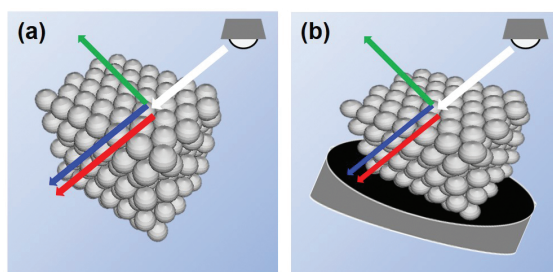


Figure 1. (a) A highly crystalline CPhC transmits light of certain wavelengths and reflects the other wavelengths. This response results in an opalescent appearance. (b) CPhCs are doped on black materials; transmitted light is absorbed, and the reflected light became more visible.

Incorporating a variety of NPs in CPhCs produces brilliant iridescent colors [20–32] because NPs can absorb and scatter visible light. In this chapter, CPhCs were incorporated directly into copper-oxide (CuO)-NPs and Ag-NPs of metal NPs by using a simple method [30, 33]. The metal NPs in the CPhC structures absorb the visible light and reduce scattering light that enhanced the color under natural lighting conditions. The method is mainly used to distribute metal NPs on PS nanosphere surfaces due to electrostatic interactions. Additionally, the sediment of metal NPs on the bottom of substrate could absorb scattering light because Cu and Ag materials are denser than PS, resulting in production of vivid structural colors. The reflection wavelengths of PS CPhC films with and without CuO-NPs and Ag-NPs were predicted theoretically and compared with the corresponding experimental results. The structural colors of the CuO-NPs/PS and Ag-NPs/PS hybrid CPhC color films were not only substantially enhanced but also varied with observation angles. CuO-NPs/PS and Ag-NPs/PS hybrid CPhCs exhibiting enhanced structural colors were obtained using a simple and inexpensive method. In addition, Cu-NPs and Ag-NPs are generally used as antimicrobial agents [34, 35] and catalysts [36, 37] in the biomedical field. Therefore, CPhCs incorporated

with CuO-NPs or Ag-NPs could provide additional advantages, such as antibacterial activity, in textile fabrics.

2. Materials and methods

2.1. Materials

Styrene (St) was distilled prior to use. Sodium dodecyl sulfate (SDS), potassium persulfate (KPS), sodium bicarbonate (NaHCO_3), Cu nanopowder (40–60 nm particle size; 99.5% trace metal basis), and Ag nanopowder (<100 nm particle size; 99.5% trace metal basis) were used as received. Deionized (DI) water (18.2 M Ω cm resistivity) was purified using a PURELAB purification system. Cover glasses (Marienfeld) with hydrophilic surface were prepared using O_2 plasma.

2.2. Synthesis of monodisperse PS nanospheres

Negatively charged PS nanospheres were synthesized via an emulsion polymerization method as described previously [28] by using St as monomer, SDS as emulsifier, KPS as initiator, and NaHCO_3 as buffer. SDS was used to render negative charge to the surface of PS nanospheres [28]. Different sizes of colloidal PS nanospheres were synthesized using the same method by varying the quantity of SDS and St. The diameter of PS nanospheres (D_{PS}) was approximately linearly dependent on the amount of SDS and St (**Figure 2(a)** and **(b)**), respectively. **Table 1** shows the structural parameters for six PS CPhCs used in this chapter. For example, the sample B synthesis process is as follows: First, 200 mL of DI water, 125 mg of NaHCO_3 , and 150 mg of SDS were mixed in a 500-mL three-necked flask, which was placed in a water bath under nitrogen protection. Then, 15 mL of St and 250 mg of KPS were added into the mixture. After stirring for 24 h, PS nanospheres with an average D_{PS} of 230 nm were obtained. Using the same synthesis process (sample E), we used 150 mg of SDS, 125 mg of NaHCO_3 , 200 mL of DI water, 250 mg of KPS dissolved in 50 mL of DI water, and 8 g of styrene to obtain a D_{PS} of 215 nm. PS nanosphere powders were purified through dialysis, collected via centrifugation at 15,000 rpm for 1 h, and purified five times by washing with DI water before drying in a vacuum oven.

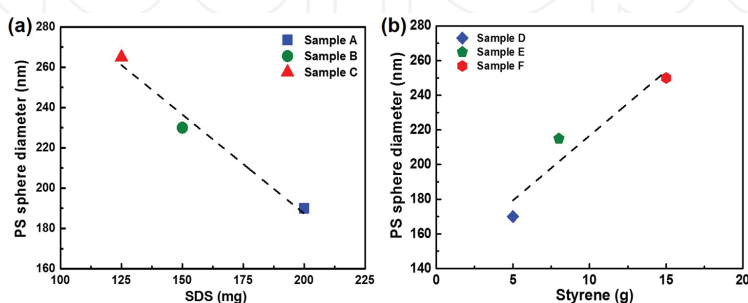


Figure 2. Diameter of colloidal PS nanospheres was dependent on the amount of (a) SDS and (b) styrene. Black dashed line indicates linear fitting.

Sample	Diameter (D_{PS} , nm)	Normal reflection peak ($\lambda_{R/}$, nm)
A	190	452
B	230	547
C	265	630
D	170	417
E	215	515
F	250	601

Table 1. Structural parameters for the six PS CPhCs used in this chapter.

2.3. Attachment of CuO-NPs and Ag-NPs onto colloidal PS latex

Cu and Ag nanopowder with 99.5% metal basis were purchased from Sigma-Aldrich. Cu-NPs are easily oxidized upon exposure to an ambient laboratory atmosphere at room temperature. We utilized the random adsorption of CuO-NPs and Ag-NPs on negatively charged PS nanospheres. PS latex suspensions of six PS CPhCs with different D_{PS} (samples A–F, **Table 1**) at a concentration of approximately 4.8 weight percent (wt%) were prepared through ultrasonication. Varying PS latex suspensions (4.8 wt%) were added with 0.05, 0.10, and 0.50 wt% Cu nanopowder, and 1.0 and 4.5 wt% Ag nanopowder. Random distribution of metal NPs on PS surfaces through electrostatic interactions was achieved by ultrasonication for 8 h; the unabsorbed metal NPs settled at the bottom of the bottle.

2.4. Preparation of CuO-NPs/PS and Ag-NPs/PS hybrid CPhC color films

CuO-NPs/PS and Ag-NPs/PS hybrid CPhC color films were fabricated by the thermal-assisted self-assembly process and the gravitational sedimentation method (**Figure 3**). 200 μ L of metal NPs/PS mixture suspensions were dropped on a cover glass. The suspension was spread to the glass surface. Then, the glass was placed in an oven at a constant temperature of 50°C for 2 h. The oven temperature was subsequently raised to 80°C for 30 min to improve the physical rigidity of the metal NPs/PS hybrid CPhC color films. Field-emission scanning electron microscopy (FESEM) was used to study the crystalline structure of the metal NPs/PS hybrid CPhC color films (**Figure 4(a)–(f)**).

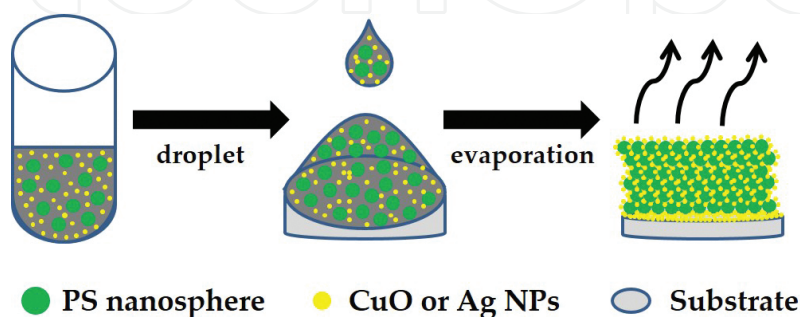


Figure 3. Schematic of the thermal-assisted self-assembly via gravitational sedimentation method.

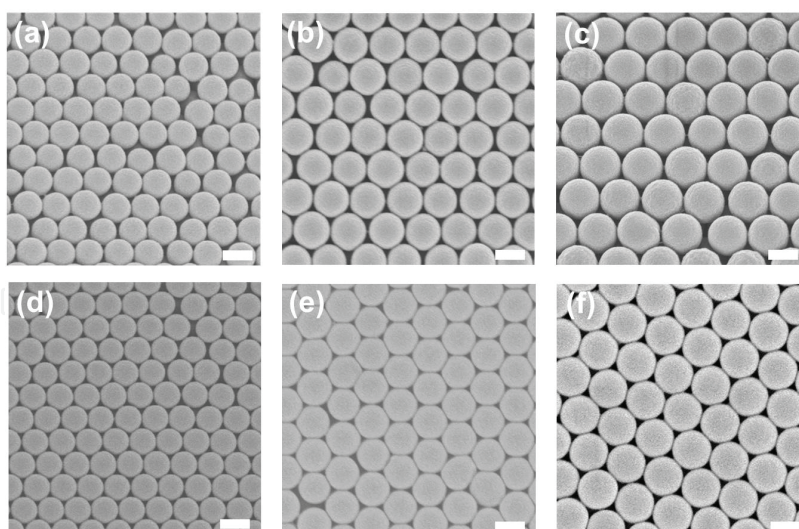


Figure 4. FESEM images of PS CPhC structures: (a) sample A, (b) sample B, (c) sample C, (d) sample D, (e) sample E, and (f) sample F. All scale bars represent 200 nm.

2.5. Characterization

The morphology of CuO-NPs/PS and Ag-NPs/PS hybrid CPhC color films was observed using FESEM (S-4800, Hitachi) and field-emission transmission electron microscope (FETEM, JEM-2100F, JEOL). Energy dispersive spectrometer (EDS, EMAX400, Horiba) was used to verify the presence of CuO-NPs and Ag-NPs on PS nanosphere surface. UV-Visible extinction spectra were obtained in standard transmittance mode, and the reflectance and color of metal NPs/PS hybrid CPhC color films were measured on a HR2000 spectrometer (Ocean Optics) with unpolarized white light provided by a Xe light source. Fiber optic Y-cables were used in reflection measurement. The color of the metal NPs/PS hybrid CPhCs color films was measured using SpectraSuite software (Ocean Optics) according to the Commission International d'Eclairage (CIE) 1931 standard colorimetric system. Raman spectra were analyzed from the reference database KnowItAll Information System (Bio-Rad Laboratories). Cover glasses (diameter, 10 mm; Marienfeld) were treated with plasma (Zepto, Diener) to obtain a hydrophilic surface before use.

3. Results

3.1. Optical properties of the CuO-NPs

Cu is the most commonly used metal in various applications in electronics due to its conductivity and low cost. As Cu is prone to oxidation, this could significantly affect the optical properties of CuO-NPs. Therefore, the optical characteristics of CuO-NPs are initially discussed in this chapter. **Figure 5** exhibits the surface adsorption of CuO-NPs on PS nanospheres which could cause visible light absorption. Furthermore, **Figure 5** demonstrates the absorbance degree of light which was dependent on the CuO-NPs content. **Figure 5(a)** shows the

black-brown color of diluted solution because visible light was absorbed by CuO-NPs. In addition, **Figure 5(c)** shows the transmittance spectra of different CuO-NP concentrations, in which the CuO-NPs were strongly absorbed in the visible light. The transmittance was approximately 6% or less depending on CuO-NP concentrations. Moreover, scattering is typically very sensitive to the aggregation state of the NPs, with the scattering contribution increases as particles further aggregate [21, 38]. **Figure 5(d)** demonstrates the extinction spectra depending on the aggregation state of CuO-NPs, which are nearly entirely caused by photon absorption. The extinction spectra in **Figure 5(b and d)** clearly show that CuO-NPs agglomerated.

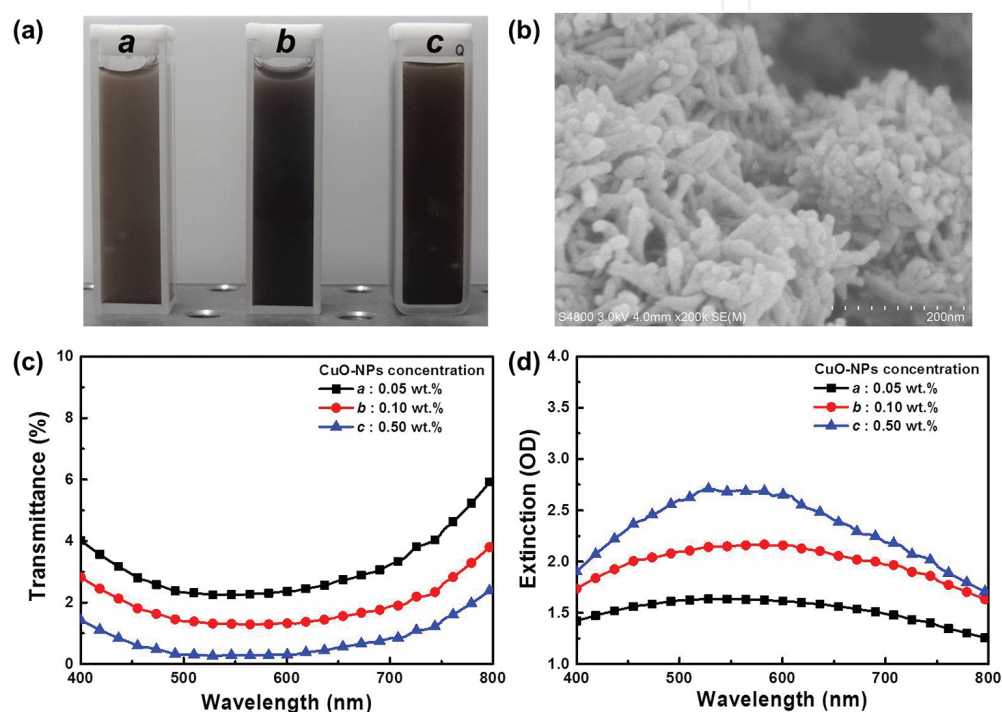


Figure 5. (a) Diluted solution appears black-brown because light is absorbed across the entire visible spectrum. (b) FESEM image of the agglomerates of 0.5 wt% CuO-NPs. (c) Transmittance and (d) extinction spectra of CuO-NP solutions resulted nearly entirely by light absorption with negligible scattering.

3.2. Optical properties of concentrated Ag-NPs

Ag-NPs are generally used for medical purposes due to its antibacterial, antimicrobial, and anti-inflammatory properties [39, 40]. In this chapter, dispersion in water could significantly affect the optical properties of concentrated Ag-NPs. Therefore, we discussed the optical characteristics of diluted Ag-NP solutions. **Figure 6(a)** shows the 1.0 and 4.5 wt% black-brown diluted solutions in a standard quartz cuvette because visible light was absorbed by Ag-NPs. FESEM images in **Figure 6(b)** demonstrated the agglomeration of Ag-NPs. The optical properties of Ag-NPs upon aggregation are affected, and conduction electrons located near each NP surface become delocalized and are shared among neighboring NPs. The extinction spectra in **Figure 6(d)** demonstrated the LSPR of Ag-NPs when they aggregated, therefore

localized surface plasmon resonance (LSPR) was not observed in this study. In addition, **Figure 6(c)** illustrates the transmittance spectra of different Ag-NP concentrations, in which strong absorption was observed in the visible spectrum. The transmittance dropped to approximately 5% or less depending on Ag-NP concentrations. **Figure 6(d)** shows the extinction spectra depending on the size, shape, and aggregation state of Ag-NPs, which are nearly entirely caused by photon absorption.

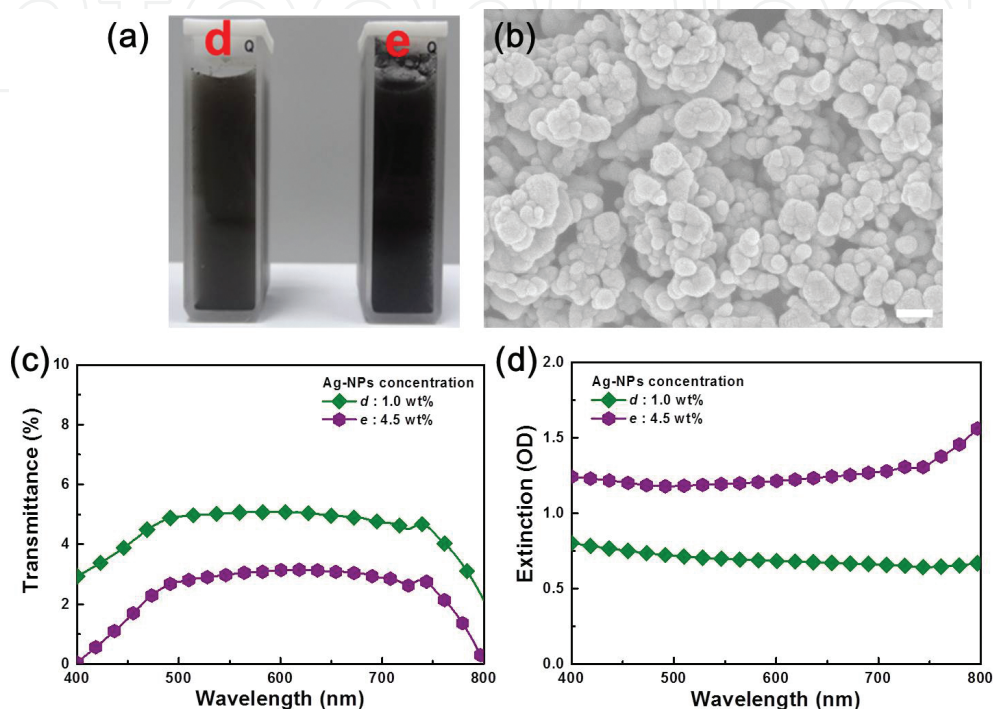


Figure 6. (a) Diluted solution appears black-brown because light is absorbed across the entire visible spectrum. (b) FESEM image of Ag-NP agglomerates at 4.5 wt% concentration. Scale bar in the inset represents 200 nm. (c) Transmittance and (d) extinction spectra of diluted Ag-NP solutions resulting nearly entirely from the absorption of all wavelengths of visible light with negligible scattering.

3.3. Crystal structures of the prepared CuO-NPs/PS hybrid CPhC color films

These studied samples contain PS nanospheres with different diameters a corresponding D_{PS} of 190, 230, and 265 nm, and different CuO-NP concentrations (samples A–C, **Table 1**). The CuO-NPs/PS hybrid CPhC color films were fabricated by mixing of CuO-NPs via a thermal-assisted self-assembly process by using a gravitational sedimentation method. FESEM was used to observe the crystalline arrangement of CuO-NPs/PS hybrid CPhC color films (**Figure 4(a)–(c)**). The CuO-NPs/PS hybrid CPhC color films exhibiting face-centered cubic (*fcc*) structures were assembled through gravitational sedimentation, and their top surfaces were parallel to the (1 1 1) crystallographic plane. **Figure 4(a)–(c)** demonstrated that the CuO-NP dopant did not disrupt the structures of CPhCs. The EDS mapping images of the CuO-NPs/PS hybrid CPhC films showed the randomly adsorbed CuO-NPs on PS nanospheres, and they appeared more often at the nanospheres compared with Cu atoms and O atoms (inset of

Figure 7); this finding indicated that surface oxidization occurred. In addition, the CuO-NPs/PS hybrid CPhC color film structures were investigated by obtaining their Raman spectra (**Figure 7**). The PS CPhC and CuO structures were measured based on their Raman spectra [41, 42] (**Figure 8**). All Raman spectra were analyzed by a commercial library search (KnowItAll Information System) and based on the literature [41, 42]. We confirmed that the doping of low CuO-NP concentrations did not affect the structural quality of the PS CPhC films.

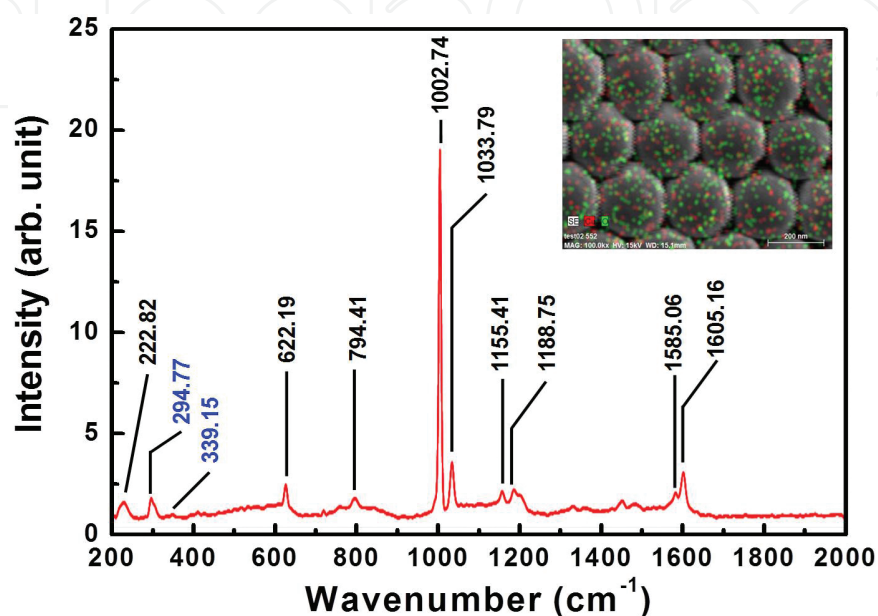


Figure 7. Raman spectrum of CuO-NPs/PS hybrid CPhC color films, in which black and blue indicate PS and CuO signals, respectively. Inset shows the EDS compositional mapping (Cu/O overlay).

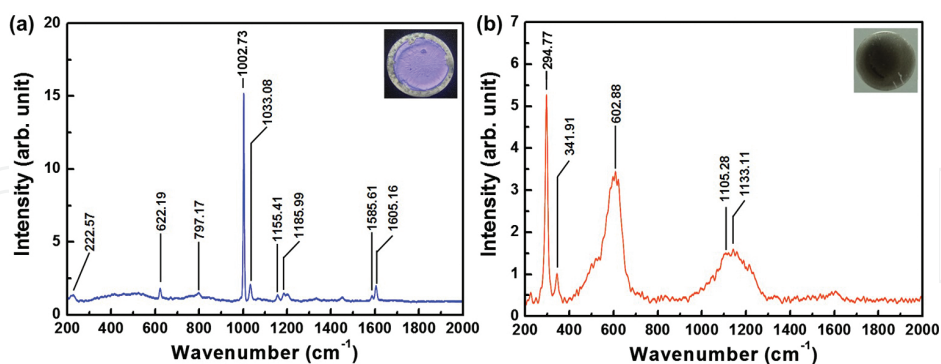


Figure 8. Raman spectrum of (a) PS CPhC and (b) CuO films. Inset shows the optical image of PS CPhC and CuO films.

3.4. Crystal structures of the prepared Ag-NPs/PS hybrid CPhC color films

Samples containing PS nanosphere with sizes (D_{PS}) of 170, 215, and 250 nm and containing various concentrations of Ag-NPs were prepared in this study (samples D–F, **Table 1**). Ag-NPs/PS hybrid CPhC color films were also fabricated by mixing Ag-NPs via a thermal-assisted

self-assembly process by using a gravitational sedimentation method. The FESEM images indicated that the Ag-NPs dopant did not disrupt the structures of CPhCs (**Figure 4(d)–(f)**). The FETEM and EDS mapping images of the Ag-NPs/PS hybrid CPhC color films showed that the Ag-NPs were randomly adsorbed on the PS nanosphere surface (**Figure 9**). **Figure 9** shows the EDS mapping images of a sample consisting of nanospheres with adsorbed Ag and O atoms. Thus, Ag-NPs easily adsorbed O atoms, indicating its antibacterial effect [43, 44]. These results suggested that introduction of high Ag-NP concentrations did not affect the structural quality of the PS CPhC films.

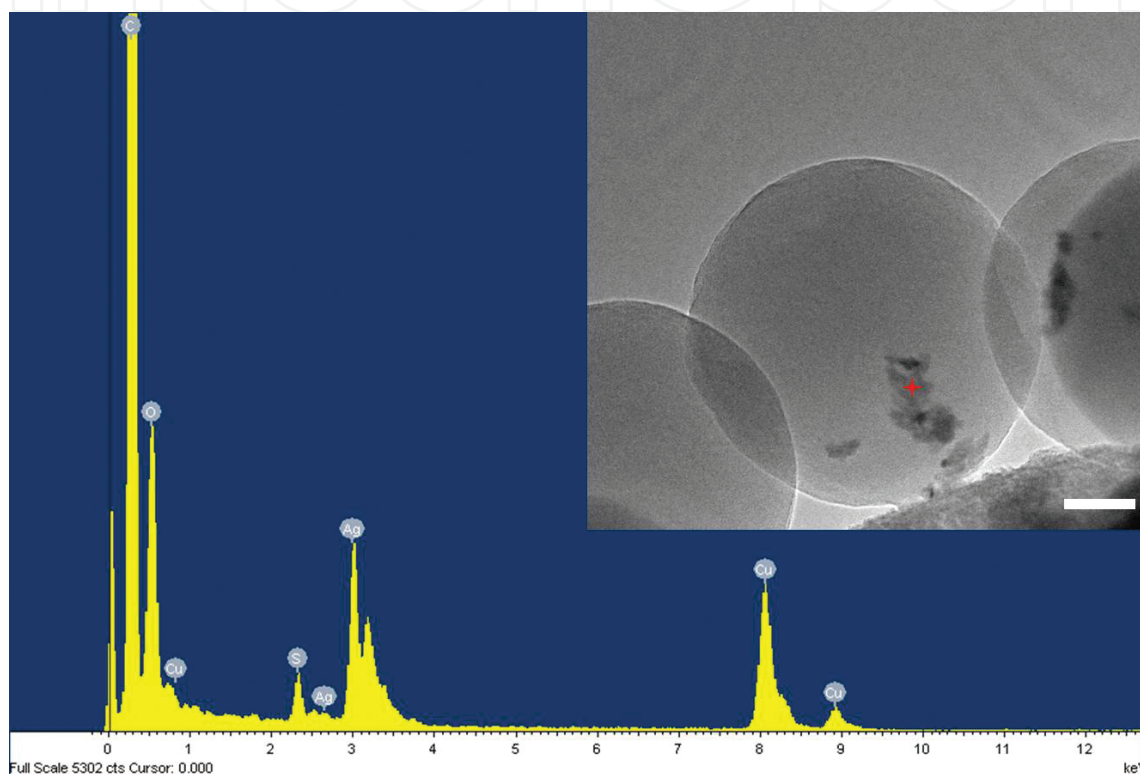


Figure 9. EDS compositional mapping (Ag) scans from the red cross point of inset FETEM image. Scale bars represent 20 nm.

3.5. Effects of CuO-NPs content on PS CPhC color films

Figure 10 shows the photographs of PS CPhCs without and with CuO-NPs. Pure PS CPhC films are usually milky white with extremely faint structural colors (**Figure 10(a)**, standard). As shown in **Figure 10(a)**, the visual appearance of metal NPs/PS hybrid CPhC color films from exhibiting dull color to vivid iridescent color clearly changed by doping CuO-NPs into PS CPhCs. These pictures were observed under a fluorescent lamp and exhibited a highly angular-dependent Bragg diffraction law. These pictures show a tunable color mechanism, which contributed to the absorbance of scattering light by doped CuO-NPs. For example, in this study was obtained by doping only 0.50 wt% CuO-NPs into PS CPhCs, and the visual appearance of hybrid CPhC color films changed evidently (**Figure 10**). Additionally, **Figure 10(b)** exhibits

the back surface photographs of CuO-NPs/PS hybrid CPhC color films. The visual appearance of the CPhC color films changes remarkably from milky white to deep brown by doping CuO-NPs into the *fcc* structure (**Figure 10(b)**, sample B). Consequently, CuO-NPs may absorb scattering light and increase color saturation, producing bright structural colors of CPhCs.

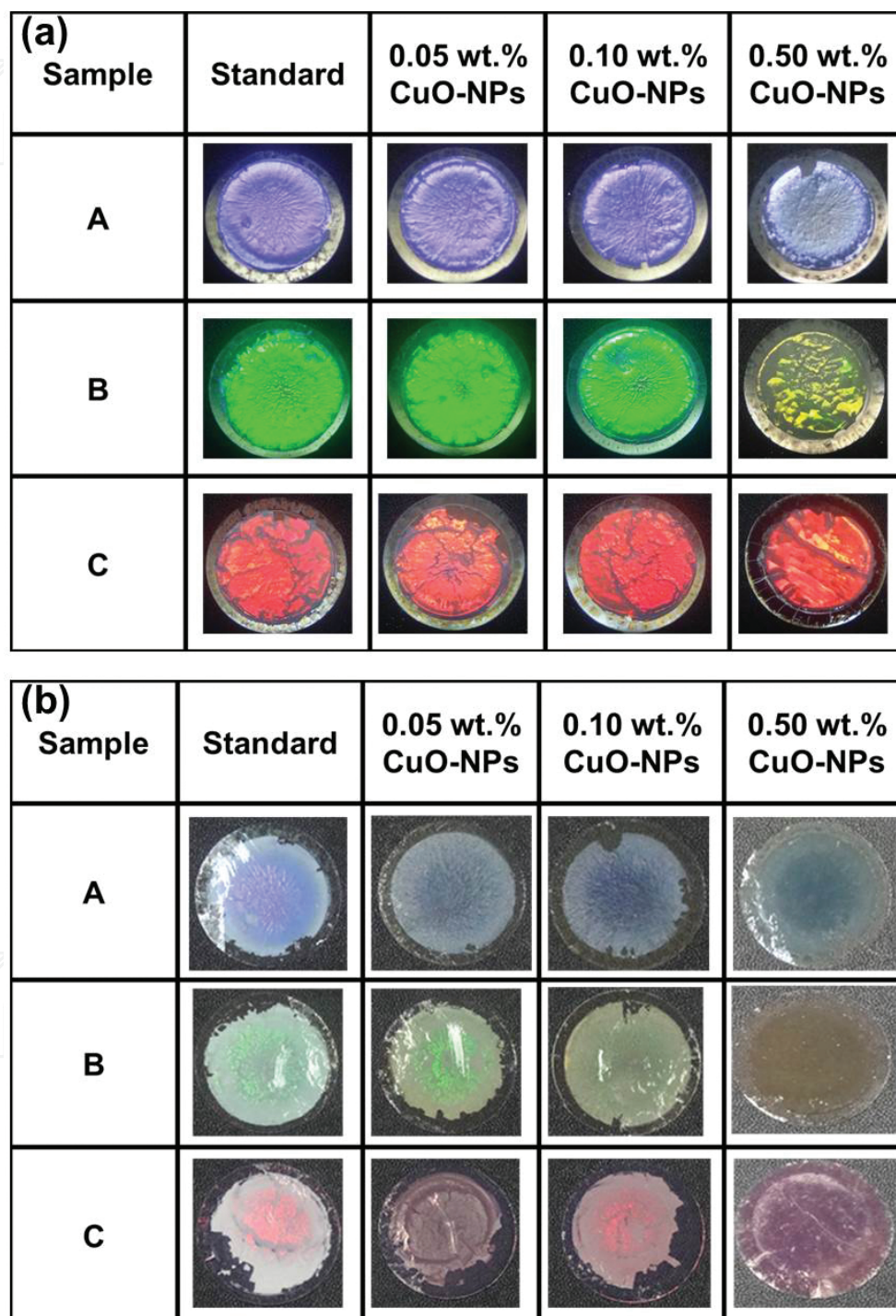


Figure 10. (a) Top surface and (b) back surface of CuO-NPs/PS hybrid CPhC color films (1) without CuO-NPs (standard), and (2) with 0.05 wt% and (3) 0.10 wt% and (4) with 0.50 wt% CuO-NPs.

3.6. Effects of Ag-NPs content on PS CPhC color films

Figure 11 shows the photographs of Ag-NPs/PS hybrid CPhC color films. Pure PS CPhC color films are generally milky white with faint structural colors (**Figure 11(a)**, standard). The visual appearance of hybrid CPhCs clearly changed from dull color to vivid iridescent color by doping Ag-NPs into PS CPhCs (**Figure 11(a)**). The pictures indicated a tunable color mechanism, which contributed to the absorbance of scattering light by doping Ag-NPs. After doping the Ag-NPs into the PS CPhCs, the visual appearance of hybrid CPhC color films changed evidently (**Figure 11(a)**). **Figure 11(b)** exhibits the back surface photographs of Ag-NPs/PS hybrid CPhC color films. The visual appearance of the hybrid CPhC color films changes quite clearly from milky white to deep green after doping Ag-NPs into the *fcc* structure (**Figure 11(b)**, sample E). Consequently, Ag-NPs may absorb scattered light and increase color saturation, producing bright structural colors of CPhCs. In addition, we observed the coffee ring of CPhC color films (**Figure 11(a)**).

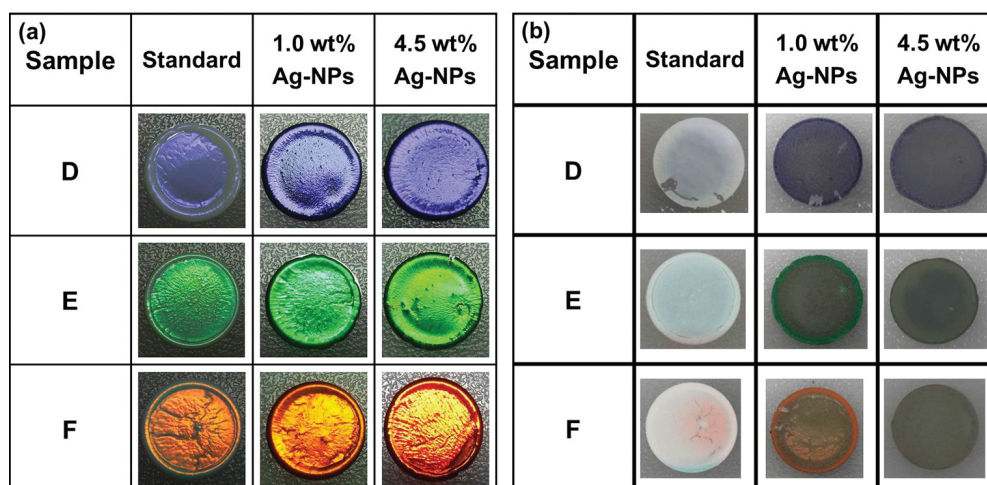


Figure 11. (a) Top surface and (b) back surface of AgNPs/PS hybrid CPhC color films (1) without AgNPs (standard) and with (2) 1.0 wt% and (3) 4.5 wt% AgNPs.

4. Discussion

The normal reflectance spectra of all samples were measured on a UV-Visible spectrometer equipped with a Xe lamp. Collimated broadband white light from a UV-enhanced Xe lamp was incident of normal surface of the sample, in which the Ag mirror as reference for reflectance measurement was the incident light of the Xe light source. The light spot size on the sample was approximately 4.0 mm. Fiber optic Y-cables were used for reflectance measurement. The theoretical reflection wavelengths of the Bragg diffraction law of metal NPs/PS hybrid CPhC color films were calculated by using the combined form of Bragg law and Snell law. According to the Bragg-Snell law Eq. (1), the relationship between the reflection peak wavelength (λ_R) and the incident angle (α) of an *fcc* structure is as follows:

$$\lambda_R = \sqrt{8/3} D_{PS} \sqrt{n_{eff}^2 - \sin^2 \alpha} \quad (1)$$

where D_{PS} is the diameter of PS nanospheres. To obtain n_{eff} which is the effective refractive index of the medium. In this case, $n_{NP_{s_air}}$ was obtained using Eq. (2), as follows:

$$n_{eff} = [n_{PS}^2 f_{PS} + n_{NP_{s_air}}^2 (1 - f_{PS})]^{1/2} \quad (2)$$

where $n_{PS} = 1.59236$ is the refractive index of PS nanospheres and $f_{PS} = 0.74$ is the volume fraction of the PS nanosphere. Therefore, we can obtain $n_{NP_{s_air}}$ which is the refractive index of NPs.

4.1. Tunable structural color of the CuO-NPs/PS CPhC color films

Figure 12(a)–(c) shows the reflectance spectra of PS CPhC color films with and without CuO-NPs. Pure PS CPhC color films exhibited the reflectance peaks at 452 (sample A), 547 (sample B), and 630 nm (sample C), corresponding to blue, green, and red, respectively. After introducing 0.50 wt% of CuO-NPs into the three kinds of PS nanospheres, the hybrid CPhC color films showed a low reflection intensity and broadband reflectance peaks at 459, 557, and 638 nm, corresponding to cyan blue, yellow, and deep red. The reflectance spectra of PS CPhCs

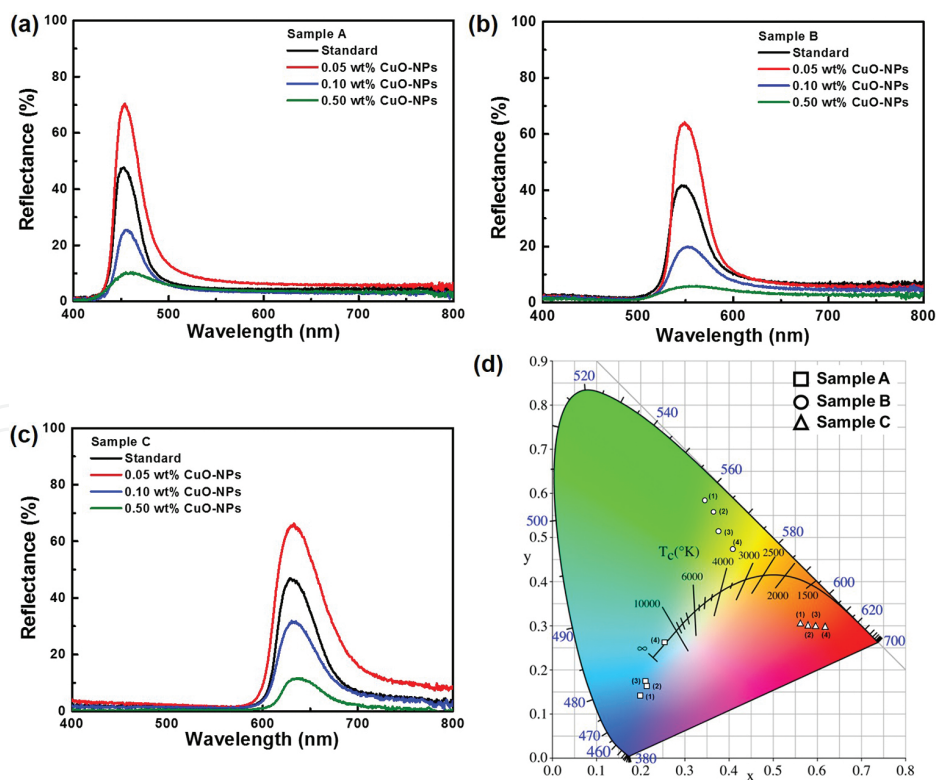


Figure 12. Reflection spectra of PS CPhC films with and without CuO-NPs: (a) sample A (\square), (b) sample B (\circ), and (c) sample C (\triangle). (d) CIE chromaticity diagram of CuO-NPs/PS hybrid CPhC color films for different samples (A–C) and CuO-NP contents.

containing various amounts of CuO-NPs showed different reflection peak positions, consistent with the Bragg law. The color of CuO-NPs/PS hybrid CPhC color films was calculated by using the corresponding chromaticity coordinates of the CIE 1931 standard colorimetric system. The visible light (380–700 nm) of the CIE 1931 chromaticity diagram visually calculated the changes in hybrid CPhC structural colors. The color of the CuO-NPs/PS hybrid CPhC color films was measured by irradiation on a D65 light source. Then, the reflection spectra obtained from CuO-NPs/PS hybrid CPhC color films were used to calculate the CIE 1931 chromaticity coordinates by using SpectraSuite software. The structural color of CPhCs was visually presented in the CIE 1931 chromaticity diagram, in which the color coordinates indicated the corresponding color. The PS nanospheres with a D_{PS} of 190 (sample A, □), 230 (sample B, O), and 265 nm (sample C, Δ), the corresponding structural colors were blue, green, and red, respectively (**Figure 12(d)**). Under the same D_{PS} , doping different CuO-NPs correspond to the same color hue but with different color purities. Three primary colors were obtained by using the CuO-NPs/PS hybrid CPhC color films, and iridescent colors were also achieved by modifying the D_{PS} of PS nanospheres (**Figure 12(d)**). Additionally, **Figure 12(d)** shows the larger color shift of sample A (□) and sample B (O) than that of sample C (Δ) because the reflection peak of sample C was considerably close to the cutoff wavelength (700 nm) of the CIE 1931 chromaticity diagram. The CuO-NPs/PS hybrid CPhC films demonstrated considerable potential to exhibit not only panchromatic colors but also holographic colors. Thus, CuO-NPs content and PS nanosphere size could influence the optical properties of CPhC color films.

4.2. Tunable structural color of the Ag-NPs/PS CPhC color films

Figure 13(a)–(c) shows the reflectance spectra of Ag-NPs/PS hybrid CPhC color films, in which the PS nanospheres with a D_{PS} were 170 (sample D), 215 (sample E), and 250 nm (sample F). Pure PS CPhC color films exhibited the reflectance peaks at 417 (sample D), 515 (sample E), and 601 nm (sample F), corresponding to blue, green, and red. After introducing 4.5 wt% of Ag-NPs into three kinds of PS CPhCs, the hybrid CPhC films showed the low reflection intensity and red-shift reflectance peaks at 421, 519, and 608 nm. The reflectance spectra of Ag-NPs/PS hybrid CPhC color films showed different reflection peak positions, consistent with the Bragg law. In addition, the PS CPhC films containing Ag-NPs exhibited weak reflectance because of the considerably high Ag-NP concentration (**Figure 13(a)–(c)**). The structural color was brilliant with the increase of Ag-NPs content, because the scattered light was strongly absorbed by the sediment on the bottom of Ag-NPs. Conversely, excessive Ag-NPs resulted in reduced reflection peak height and loss of brightness. Therefore, more photons could absorb in the PBG. The structural color of CPhC color films was effectively enhanced by introducing an appropriate amount of Ag-NPs. The effects of Ag-NPs content on the structural color of CPhC color films are summarized in **Figure 13(d)**.

The structural colors of Ag-NPs/PS hybrid CPhC films were calculated by using the corresponding chromaticity coordinates of the CIE 1931 standard colorimetric system. The visible light (380–700 nm) of the CIE 1931 chromaticity diagram visually calculated the changes in CPhC structural colors. Structural color of Ag-NPs/PS hybrid CPhC color films was measured by irradiating under a D65 light source. The reflection spectra of Ag-NPs/PS hybrid CPhC color

films were used to determine CIE 1931 chromaticity coordinates. The structural color of hybrid CPhCs was visually presented in the CIE 1931 chromaticity diagram, in which the color coordinates indicated the corresponding structural color. At PS nanospheres with D_{PS} of 170 (sample D, \diamond), 215 (sample E, \square), and 250 nm (sample F, \square), the structural colors were blue, green, and red, respectively (**Figure 13(d)**). Under the same D_{PS} , introducing different Ag-NPs corresponds to the same color hue but with different purities. The three primary colors were obtained by using the AgNPs/PS hybrid CPhC films, and iridescent colors were obtained by altering the D_{PS} (**Figure 13(d)**). Additionally, **Figure 13(d)** exhibits slight color shifts for samples D (\diamond), E (\square), and F (\square). The Ag-NPs/PS hybrid CPhC color films demonstrated a considerable potential to show not only panchromatic colors but also holographic colors. Thus, PS nanosphere size and Ag-NP content could influence the optical properties of CPhC color films.

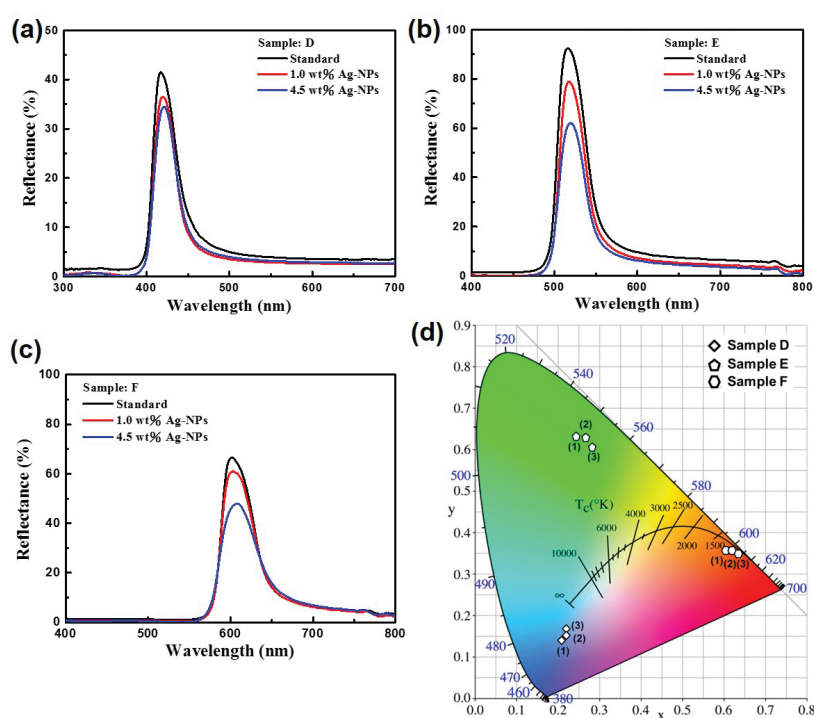


Figure 13. Reflection spectra of PS CPhC films with and without Ag-NPs: (a) sample D (\diamond), (b) sample E (\square), and (c) sample F (\square). (d) CIE chromaticity diagram of Ag-NPs/PS hybrid CPhC color films for different samples (D–F) and Ag-NP contents.

5. Conclusion

In this chapter, CuO-NPs and Ag-NPs doped into PS CPhC structures could absorb all wavelengths, remarkably increasing the color and producing brilliant tunable structural colors that are visible under natural lighting conditions. Considering that backscattered light was absorbed by the embedded metal NPs, the visual appearance of colloidal crystal coatings changed markedly from faint milky white to brilliant colors. The experimental results

confirmed that introduction of low CuO-NP concentrations and high Ag-NP concentrations did not affect the structural quality of the PS CPhC films. In addition, the NPs/PS hybrid CPhC color films were measured and predicted by UV-Visible spectroscopy, FESEM, and EDS. The measured PBGs of the CPhCs were consistent with the theoretical calculation. The proposed novel method allows acquisition of tunable structural color for future applications in textile fabrics, bionic colors, catalysis, and paints.

Acknowledgements

This work is supported by the Ministry of Science and Technology (MOST) in Taiwan, under contract numbers MOST103-2221-E-035-029, and MOST105-2221-E-035-041. The authors appreciate the Precision Instrument Support Center of Feng Chia University for providing the fabrication and measurement facilities.

Author details

Chun-Feng Lai

Address all correspondence to: chunflai@fcu.edu.tw

Department of Photonics, Feng Chia University, Seatwen, Taichung, Taiwan

References

- [1] M. Srinivasarao. Nano-optics in the biological world: beetles, butterflies, birds, and moths. *Chem. Rev.* 1999;99(7):1935–1961. DOI: 10.1021/cr970080y.
- [2] P. Vukusic, and J. R. Sambles. Photonic structures in biology. *Nature.* 2003;424:852–855. DOI: 10.1038/nature01941
- [3] R. A. Potyrailo, H. Ghiradella, A. Vertiatchikh, K. Dovidenko, J. R. Cournoyer, and E. Olson. Morpho butterfly wing scales demonstrate highly selective vapour response. *Nat. Photon.* 2007;1:123–128. DOI: 10.1038/nphoton.2007.2
- [4] J. D. Forster, H. Noh, S. F. Liew, V. Saranathan, C. F. Schreck, L. Yang, J. G. Park, R. O. Prum, S. G. J. Mochrie, C. S. O'Hern, H. Cao, and E. R. Dufresne. Biomimetic isotropic nanostructures for structural coloration. *Adv. Mater.* 2010;22:2939–2944. DOI: 10.1002/adma.200903693
- [5] Y. Takeoka. Angle-independent structural coloured amorphous arrays. *J. Mater. Chem.* 2012;22:23299–23309. DOI: 10.1039/C2JM33643J

- [6] H. Noh, S. F. Liew, V. Saranathan, S. G. J. Mochrie, R. O. Prum, E. R. Dufresne, and H. Cao. How noniridescent colors are generated by quasi-ordered structures of bird feathers. *Adv. Mater.* 2010;22:2871–2880. DOI: 10.1002/adma.200903699
- [7] C. F. Lai, Y. C. Wang, and H. C. Hsu. High transparency in the structural color resin films through quasi-amorphous arrays of colloidal silica nanospheres. *J. Mater. Chem. C.* 2016;4:398–406. DOI: 10.1039/C5TC03063C
- [8] H. Cong, B. Yu, J. Tang, Z. Li, and X. Liu. Current status and future developments in preparation and application of colloidal crystals. *Chem. Soc. Rev.* 2013;42:7774–7800.
- [9] A. Stein, B. E. Wilson, and S. G. Rudisill. Design and functionality of colloidal-crystal-templated materials-chemical applications of inverse opals. *Chem. Soc. Rev.* 2013;42:2763–2803.
- [10] N. Vogel, M. Retsch, C. -A. Fustin, A. d. Campo, and U. Jonas. Advances in colloidal assembly: the design of structure and hierarchy in two and three dimensions. *Chem. Rev.* 2015;115(13):6265–6311. DOI: 10.1021/cr400081d
- [11] C. I. Aguirre, E. Reguera, and A. Stein. Tunable colors in opals and inverse opal photonic crystals. *Adv. Funct. Mater.* 2010;20:2565–2578. DOI: 10.1002/adfm.201000143
- [12] Y. Li, G. Duan, G. Liu, and W. Cai. Physical processes-aided periodic micro/nanostructured arrays by colloidal template technique: fabrication and applications. *Chem. Soc. Rev.* 2013;42:3614–3627.
- [13] C. F. Lai, Y. C. Lee, and T. L. Tsai. Candlelight LEDs fabricated by using composite silica photonic crystals. *Opt. Mater. Express.* 2015;5(2):307–313. DOI: 10.1364/OME.5.000307
- [14] C. F. Lai, Y. C. Lee, and C. T. Kuo. Saving phosphor by 150% and producing high color-rendering index candlelight LEDs containing composite photonic crystals. *J. Light. Technol.* 2014;32(10):1930–1935. DOI: 10.1109/JLT.2014.2309955
- [15] S. M. Klein, V. N. Manoharan, D. J. Pine, and F. F. Lange. Preparation of monodisperse PMMA microspheres in nonpolar solvents by dispersion polymerization with a macromonomeric stabilizer. *Colloid Polym. Sci.* 2003;282(1):7–13. DOI: 10.1007/s00396-003-0915-0
- [16] Y. Zhang, B. Dong, A. Chen, X. Liu, L. Shi, and J. Zi. Using cuttlefish ink as an additive to produce non-iridescent structural colors of high color visibility. *Adv. Mater.* 2015;27(32):4719–4724. DOI: 10.1002/adma.201501936
- [17] B. Tang, Y. Xu, T. Lin, and S. Zhang. Polymer opal with brilliant structural color under natural light and white environment. *J. Mater. Res.* 2015;30(20):3134–3141. DOI: <http://dx.doi.org/10.1557/jmr.2015.238>
- [18] F. Wang, Z. Gou, Y. Ge, and K. An. Preparation of tunable structural colour film by coating ps with titania on glass. *IET Micro Nano Lett.* 2016;11(1):50–53. DOI: 10.1049/mnl.2015.0264

- [19] F. Wang, X. Zhang, L. Zhang, M. Cao, Y. Lin, and J. Zhu. Rapid fabrication of angle-independent structurally colored films with a superhydrophobic property. *Dyes Pigment*. 2016;130:202–208. DOI: 10.1016/j.dyepig.2016.03.022
- [20] H. Cong, B. Yu, S. Wang, L. Qi, J. Wang, and Y. Ma. Preparation of iridescent colloidal crystal coatings with variable structural colors. *Opt. Express*. 2013;21(15):17831–17838. DOI: 10.1364/OE.21.017831
- [21] C. I. Aguirre, E. Reguera, and A. Stein. Colloidal photonic crystal pigments with low angle dependence. *ACS Appl. Mater. Interf.* 2010;2(11):3257–3262. DOI: 10.1021/am100704f
- [22] Z. Shen, L. Shi, B. You, L. Wu, and D. Zhao. Large-scale fabrication of three-dimensional ordered polymer films with strong structure colors and robust mechanical properties. *J. Mater. Chem.* 2012;22:8069–8075. DOI: 10.1039/C2JM30546A
- [23] W. Wang, B. Tang, W. Ma, J. Zhang, B. Ju, and S. Zhang. Easy approach to assembling a biomimetic color film with tunable structural colors. *J. Opt. Soc. Am. A*. 2015;32(6):1109–1117. DOI: 10.1364/JOSAA.32.001109
- [24] O. L. J. Pursiainen, J. J. Baumberg, H. Winkler, B. Viel, P. Spahn, T. Ruhl. Nanoparticle-tuned structural color from polymer opals. *Opt. Express*. 2007;15(15):9553–9561. DOI: 10.1364/OE.15.009553
- [25] Y. Yamada, M. Ishii, T. Nakamura, and K. Yano. Artificial black opal fabricated from nanoporous carbon spheres. *Langmuir*. 2010;26(12):10044–10049. DOI: 10.1021/la1001732
- [26] F. Wang, X. Zhang, Y. Lin, L. Wang, and J. Zhu. Structural coloration pigments based on carbon modified ZnS@SiO₂ nanospheres with low-angle dependence, high color saturation, and enhanced stability. *ACS Appl. Mater. Interf.* 2016;8(7):5009–5016. DOI: 10.1021/acsami.5b11919
- [27] F. Wang, X. Zhang, Y. Lin, L. Wang, Y. Qin, and J. Zhu. Fabrication and characterization of structurally colored pigments based on carbon-modified ZnS nanospheres. *J. Mater. Chem. C*. 2016;4:3321–3327. DOI: 10.1039/C5TC04192A
- [28] M. O. A. Erola, A. Philip, T. Ahmed, S. Suvanto, and T. T. Pakkanen. Fabrication of Au- and Ag-SiO₂ inverse opals having both localized surface plasmon resonance and Bragg diffraction. *J. Solid State Chem.* 2015;230:209–217. DOI: 10.1016/j.jssc.2015.06.036
- [29] B. Yu, F. Zhai, H. Cong, and D. Yang. Photosensitive polystyrene/silver bromide hybrid colloidal crystals as recoverable colorimetric naked eye probes for bromine gas sensing. *J. Mater. Chem. C*. 2016;4:1386–1391. DOI: 10.1039/C5TC02616D
- [30] C. F. Lai, Y. C. Wang, C. L. Wu, J. Y. Zeng, and C. F. Lin. Preparation of a colloidal photonic crystal containing CuO nanoparticles with tunable structural colors. *RSC Adv.* 2015;5:105200–105205. DOI: 10.1039/C5RA21035F

- [31] Z. Mu, X. Zhao, Y. Huang, M. Lu, and Z. Gu. Photonic crystal hydrogel enhanced plasmonic staining for multiplexed protein analysis. *Small*. 2015;11:6036–6043. DOI: 10.1002/sml.201501829
- [32] X. Zhao, J. Xue, Z. Mu, Y. Huang, M. Lu, and Z. Gu. Gold nanoparticle incorporated inverse opal photonic crystal capillaries for optofluidic surface enhanced Raman spectroscopy. *Biosens. Bioelectron.* 2015;72:268–274. DOI: 10.1016/j.bios.2015.05.036
- [33] C. F. Lai, and Y. C. Wang. Colloidal photonic crystals containing silver nanoparticles with tunable structural colors. *Crystals*. 2016;6(5):61. DOI: 10.3390/cryst6050061
- [34] J. P. Ruparelia, A. K. Chatterjee, S. P. Duttgupta, and S. Mukherji. Strain specificity in antimicrobial activity of silver and copper nanoparticles. *Acta Biomaterialia*. 2008;4(3): 707–716. DOI: 10.1016/j.actbio.2007.11.006
- [35] I. Sondi, and B. S. Sondi. Silver nanoparticles as antimicrobial agent: a case study on *E. coli* as a model for Gram-negative bacteria. *J. Colloid Inter. Sci.* 2004;275(1):177–182. DOI: 10.1016/j.jcis.2004.02.012
- [36] A. J. Vizcaino, A. Carrero, and J. A. Calles. Hydrogen production by ethanol steam reforming over Cu–Ni supported catalysts. *Int. J. Hydrogen Energy*. 2007;32(10–11): 1450–1461. DOI: 10.1016/j.ijhydene.2006.10.024
- [37] S. Ashokkumar, S. Ravi, V. Kathiravan, and S. Velmurugan. Synthesis, characterization and catalytic activity of silver nanoparticles using *Tribulus terrestris* leaf extract. *Spectrochim. Acta Mol. Biomol. Spectrosc.* 2014;121:88–93. DOI: 10.1016/j.saa.2013.10.073
- [38] G. H. Chan, J. Zhao, E. M. Hicks, G. C. Schatz, and R. P. V. Duyne. Plasmonic properties of copper nanoparticles fabricated by nanosphere lithography. *Nano Lett.* 2007;7(7): 1947–1952. DOI: 10.1021/nl070648a
- [39] A. Haider, and I. K. Kang. Preparation of silver nanoparticles and their industrial and biomedical applications: a comprehensive review. *Adv. Mater. Sci. Engine.* 2015;2015:165257, <http://dx.doi.org/10.1155/2015/165257>.
- [40] J. G. O. Mendoza, A. P. Vivanco, C. T. Quitl, P. Z. Moran, D. V. Hernandez, and F. Chavez. Optical fiber sensor based on localized surface plasmon resonance using silver nanoparticles photodeposited on the optical fiber end. *Sensors*. 2014;14:18701–18710. DOI: 10.3390/s141018701
- [41] M. Balkanski, M. A. Nusimovici, and J. Reydellet. First order Raman spectrum of Cu_2O . *Solid State Commun.* 1969;7(11):815–818. DOI: 10.1016/0038-1098(69)90768-6
- [42] W. T. Yao, S. H. Yu, Y. Zhou, J. Jiang, Q. S. Wu, L. Zhang, and J. Jiang. Formation of uniform CuO nanorods by spontaneous aggregation: selective synthesis of CuO , Cu_2O , and Cu nanoparticles by a solid-liquid phase arc discharge process. *J. Phys. Chem. B*. 2005;109(29):14011–14016. DOI: 10.1021/jp0517605

- [43] A. Henglein. Colloidal silver nanoparticles: photochemical preparation and interaction with O_2 , CCl_4 , and some metal ions. *Chem. Mater.* 1998;10(1):444–450. DOI: 10.1021/cm970613j
- [44] S. Pal, Y. K. Tak, and J. M. Song. Does the antibacterial activity of silver nanoparticles depend on the shape of the nanoparticle? A study of the gram-negative bacterium *Escherichia coli*. *Appl. Environ. Microbiol.* 2007;73(6):1712–1720. DOI: 10.1128/AEM.02218-06

IntechOpen

